Article

Polyunsaturated Docosahexaenoic vs Docosapentaenoic AcidDifferences in Lipid Matrix Properties from the Loss of One Double Bond

Nadukkudy V. Eldho, Scott E. Feller, Stephanie Tristram-Nagle, Ivan V. Polozov, and Klaus Gawrisch

J. Am. Chem. Soc., **2003**, 125 (21), 6409-6421• DOI: 10.1021/ja029029o • Publication Date (Web): 02 May 2003

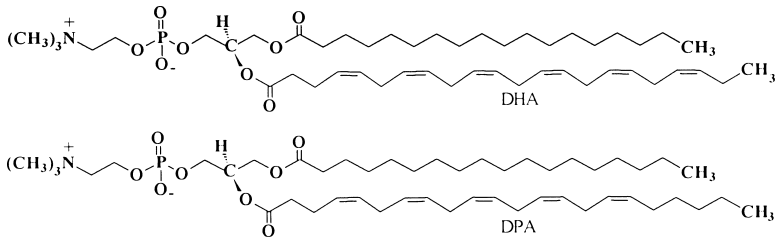

More About This Article

Additional resources and features associated with this article are available within the HTML version:

- Supporting Information
- Links to the 6 articles that cite this article, as of the time of this article download
- Access to high resolution figures
- Links to articles and content related to this article
- Copyright permission to reproduce figures and/or text from this article

View the Full Text HTML

J|A|C|S
ARTICLES
Published on Web 05/02/2003

Polyunsaturated Docosahexaenoic vs Docosapentaenoic Acid—Differences in Lipid Matrix Properties from the Loss of One Double Bond

Nadukkudy V. Eldho,[†] Scott E. Feller,[‡] Stephanie Tristram-Nagle,[§] Ivan V. Polozov,[†] and Klaus Gawrisch*,[†]

Contribution from the Laboratory of Membrane Biochemistry and Biophysics, National Institute on Alcohol Abuse and Alcoholism, National Institutes of Health, Rockville, Maryland 20852, Department of Chemistry, Wabash College, Crawfordsville, Indiana 47933, and Department of Physics, Carnegie Mellon University, Pittsburgh, Pennsylvania 15213

Received October 21, 2002; E-mail: Gawrisch@helix.nih.gov

Abstract: Insufficient supply to the developing brain of docosahexaenoic acid (22:6n3, DHA), or its ω-3 fatty acid precursors, results in replacement of DHA with docosapentaenoic acid (22:5n6, DPA), an ω-6 fatty acid that is lacking a double bond near the chain's methyl end. We investigated membranes of 1-stearoyl(d_{35})-2-docosahexaenoyl-sn-glycero-3-phosphocholine and 1-stearoyl(d_{35})-2-docosapentaenoyl-sn-glycero-3-phosphocholine by solid-state NMR, X-ray diffraction, and molecular dynamics simulations to determine if the loss of this double bond alters membrane physical properties. The low order parameters of polyunsaturated chains and the NMR relaxation data indicate that both DHA and DPA undergo rapid conformational transitions with correlation times of the order of nanoseconds at carbon atom C_2 and of picoseconds near the terminal methyl group. However, there are important differences between DHA- and DPA-containing lipids: the DHA chain with one additional double bond is more flexible at the methyl end and isomerizes with shorter correlation times. Furthermore, the stearic acid paired with the DHA in mixed-chain lipids has lower order, in particular in the middle of the chain near carbons C_{10-12}, indicating differences in the packing of hydrocarbon chains. Such differences are also reflected in the electron density profiles of the bilayers and in the simulation results. The DHA chain has a higher density near the lipid—water interface, whereas the density of the stearic acid chain is higher in the bilayer center. The loss of a single double bond from DHA to DPA results in a more even distribution of chain densities along the bilayer normal. We propose that the function of integral membrane proteins such as rhodopsin is sensitive to such a redistribution.

Introduction

Docosahexaenoic acid (22:6n3, DHA) is a common polyunsaturated fatty acid found in high concentration in the cerebral frontal cortex of mammals.[1] In synaptosomes and retinal rod outer segment (ROS) disks, and also in sperm, up to 50% of all phospholipid acyl chains are DHA.[1−4] The docosahexaenoic acid, essential for proper development of the brain,[5] is either taken up directly from food sources, such as fish, or is synthesized from ω-3 fatty acid precursors. An elaborate biochemical repair mechanism exists that replaces oxidized DHA and retains it in the brain once it has been acquired. Numerous nutritional studies have related dietary DHA content to cognitive function. Deficiencies in the supply of ω-3 fatty acids of mammals result in poor brightness-discrimination ability,[6] poor performance in shock-avoidance tasks,[7] poor exploratory behavior,[8] and poor maze performance.[9] In controlled dietary experiments adequate DHA supply improved visual acuity tasks,[10−12] visual recognition memory,[13] developmental quotient scores,[14] and the mental developmental index.[15] The precise mechanism of DHA action on brain function is

[†] Laboratory of Membrane Biochemistry and Biophysics, National Institute on Alcohol Abuse and Alcoholism, National Institutes of Health.
[‡] Department of Chemistry, Wabash College.
[§] Department of Physics, Carnegie Mellon University.

(1) Salem, N., Jr.; Kim, H. Y.; Yergey, J. A. In *Health Effects of Polyunsaturated Fatty Acids in Seafoods*; Simopoulos, A. P., Kifer, R. R., Martin, R. E., Eds. Academic Press: New York, 1986; pp 319−351.
(2) Breckenridge, W. C.; Gombos, G.; Morgan, I. G. *Biochim. Biophys. Acta* **1972**, *266*, 695−707.
(3) Neill, A. R.; Masters, C. J. *J. Reprod. Fertil.* **1973**, *34*, 279−287.
(4) Wiegand, R. D.; Anderson, R. E. *Exp. Eye Res.* **1983**, *37*, 159−173.
(5) Salem, N., Jr.; Abood, L. G.; Hoss, W. *Anal. Biochem.* **1976**, *76*, 407−415.
(6) Yamamoto, N.; Hashimoto, A.; Takemoto, Y.; Okuyama, H.; Nomura, M.; Kitajima, R.; Togashi, T.; Tamai, Y. *J. Lipid Res.* **1988**, *29*, 1013−1021.
(7) Umezawa, M.; Ohta, A.; Tojo, H.; Yagi, H.; Hosokawa, M.; Takeda, T. *Brain Res.* **1995**, *669*, 225−233.
(8) Enslen, M.; Milon, H.; Malnoe, A. *Lipids* **1991**, *26*, 203−208.
(9) Nakashima, Y.; Yuasa, S.; Hukamizu, Y.; Okuyama, H.; Ohhara, T.; Kameyama, T.; Nabeshima, T. *J. Lipid Res.* **1993**, *34*, 239−247.
(10) Birch, E. E.; Birch, D. G.; Hoffman, D. R.; Uauy, R. *Invest. Ophth. Vis. Sci.* **1992**, *33*, 3242−3253.
(11) Carlson, S. E.; Werkman, S. H.; Rhodes, P. G.; Tolley, E. A. *Am. J. Clinic. Nutr.* **1993**, *58*, 35−42.
(12) Makrides, M.; Neumann, M.; Simmer, K.; Pater, J.; Gibson, R. *Lancet* **1995**, *345*, 1463−1468.
(13) Carlson, S. E.; Werkman, S. H. *Lipids* **1996**, *31*, 85−90.
(14) Agostoni, C.; Trojan, S.; Bellu, R.; Giovannini, M. *Pediatr. Res.* **1995**, *38*, 262−266.
(15) Birch, E. E.; Garfield, S.; Hoffman, D. R.; Uauy, R.; Birch, D. G. *Devel. Med. Child Neurol.* **2000**, *42*, 174−181.

unknown. However, because of the high DHA content in synaptosomal and retinal membranes, an influence on brain function via the properties of the lipid matrix appears likely.

Insufficient supply of DHA or its ω-3 fatty acid precursors during infancy results in replacement of DHA by docosapentaenoic acid (22:5n6, DPA), an ω-6 fatty acid with the same number of carbon atoms but one fewer double bond at the terminal methyl end of the chain. This substitution is generally nonlethal, but is associated with some loss of brain function.[1,16,17] The present study was driven by the hypothesis that replacement of DHA by DPA alters the properties of neural membranes that in turn alter the function of integral receptor proteins (e.g., rhodopsin). An alternative possibility is that structural differences between DHA and DPA affect the function of peripheral enzymes involved in lipid synthesis. For example, recent studies have established that the levels of DHA in membranes are tightly linked to the accumulation of lipids with phosphatidylserine (PS) headgroups.[18] Changes in membrane protein function could then be a consequence of different PS content. Both hypotheses have in common that structural differences between DHA and DPA, and, perhaps, differences in membrane properties related to replacement of DPA by DHA are the trigger of events.

Experiments were conducted on model membranes of 1-stearoyl(d_{35})-2-docosahexaenoyl-sn-glycero-3-phosphocholine (18:0(d_{35})-22:6n3PC) or 1-stearoyl(d_{35})-2-docosapentaenoyl-sn-glycero-3-phosphocholine (18:0(d_{35})-22:5n6PC) at full hydration. The perdeuterated stearic acid chain in both lipids permitted measurement of ^{2}H NMR order parameters. In magic angle spinning NMR experiments, we resolved a large number of proton and carbon resonances of the polyunsaturated chains. The measurement of proton NOESY cross-relaxation rates provided a measure of motional and conformational disorder in the polyunsaturated membranes. The differences in motional correlation times along the polyunsaturated chain were evaluated by an analysis of ^{13}C-spin−lattice relaxation times. Chain order in the polyunsaturated chains was evaluated by measurement of the time constants for magnetization transfer from protons to carbons. The area per lipid molecule, the bilayer thickness, and the electron density profiles of the membranes were determined by X-ray diffraction. A detailed analysis of polyunsaturated chain conformation and flexibility as well as of lipid packing was achieved by comparison of experimental properties with results of molecular dynamics (MD) simulations.

Materials and Methods

Materials. Docosapentaenoic acid was purified by fractional distillation and HPLC from a mixture of fatty acid ethyl esters kindly provided by the Nutrasweet Kelco Company (Deerfield, IL). The DPA had a purity of 98 wt % as determined by gas chromatography. The phospholipids were synthesized by Avanti Polar Lipids, Inc. (Alabaster, AL).

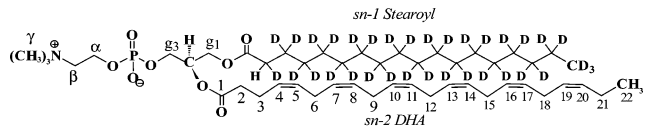

1-stearoyl(d_{35})-2-docosahexaenoyl-*sn*-glycero-3-phosphocholine (18:0(d_{35})-22:6n3PC)

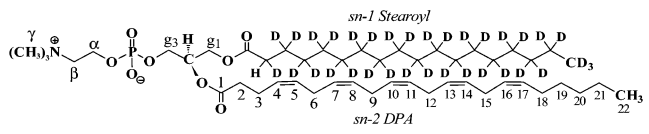

1-stearoyl(d_{35})-2-docosapentaenoyl-*sn*-glycero-3-phosphocholine (18:0(d_{35})-22:5n6PC)

Lipid purity as determined by HPLC and GC was 98%. The impurities were trace amounts of phosphatidylcholines with a different composition of fatty acids. Both lipids had a low degree of acyl chain migration (about 3% as determined by NMR). The antioxidant 2,6-di-*tert*-butyl-4-methylphenol (BHT) was added to the solution of lipids in dichloromethane at a BHT/lipid ratio of 1/250 to prevent oxidation. A quantitative assessment of the amount of oxidized lipid was conducted by GC analysis in which the peak ratios of stearic acid to DHA or DPA were compared. The content of oxidized fatty acids was below the detection level of 1%.

NMR Samples. The NMR samples were prepared in a glovebox (Plas Labs, Lansing, MI) filled with a 90/10 vol % nitrogen/hydrogen gas mixture. Residual oxygen was burned catalytically to keep the oxygen concentration below 0.1 vol % and the resulting water vapor adsorbed by a column. Carefully degassed, deuterium-depleted water or D_2O (Cambridge Isotope Laboratories, Woburn, MA) containing 1 mM diethylenetriaminepentaacetic acid (DTPA) as chelator was added to the dry lipid for a total water content of 50 wt %. The lipid/water dispersions were homogenized by stirring and centrifugation and then transferred by centrifugation into a 4-mm MAS rotor equipped with inserts made of Kel-F with a spherical sample volume of 11 μL (Bruker Instruments, Inc., Billerica, MA) or into small glass containers that were sealed with ground glass stoppers covered with a thin layer of Teflon grease. We checked the degree of lipid oxidation qualitatively by ^{1}H MAS NMR while conducting experiments, and quantitatively by GC analysis at the end of each experiment. Most samples showed insignificant amounts of oxidation (less than 1%) for periods as long as two weeks. However, samples degraded rapidly after detection of the first traces of oxidation. Results from samples that contained more than 2% of oxidized lipid were discarded.

X-ray Diffraction Samples: Oriented Samples. The lipid samples consisted of a thin (3 μm) film of lipid deposited onto a piece of freshly cleaved mica using the rock and roll method[19] to orient the approximately 500 bilayers. The originally flat mica substrate was then bent and glued to a cylindrical beaker of radius 17.5 mm. The procedure was carried out in a glovebox under exclusion of oxygen to prevent DHA/DPA oxidation. The samples were quickly inserted into the X-ray hydration chamber, and the chamber was flushed with nitrogen for 3−5 min. Hydration was accomplished in less than 40 min using a Peltier cooler to condense water onto the sample.[19]

Capillary Samples. X-ray samples in capillaries containing lipid and deionized water at a ratio of 1:1 (w,w) were prepared by the same method as the NMR samples. Capillaries were filled in an oxygen-free atmosphere, sealed with Parafilm, and flame-sealed outside the glovebox.

^{31}P NMR: The ^{31}P NMR spectra, recorded at 121.5 MHz, were acquired with a Hahn echo (d_1- 90°-τ-180°-acquire) pulse sequence with a repetition time $d_1 = 2$ s, a 3.5-μs 90° pulse, an echo delay time $\tau = 50$ μs, a spectral width of 200 kHz, and 20 kHz proton noise decoupling that was turned on at the first ^{31}P pulse of the sequence.

^{2}H NMR: Deuterium NMR spectra were observed at 46.1 MHz using a quadrupolar echo pulse sequence (d_1- 90^0_x-τ-90^0_y-acquire) with a repetition time $d_1 = 0.5$ s, a 2.7-μs 90° pulse, a delay time $\tau = 50$ μs, and a spectral width of 200 kHz. Spectra were recorded over the temperature range from −20 to +70 °C. Sample temperature was controlled to ±0.1 °C with a Bruker B-VT2000 digital temperature

(16) Salem, N. In *Current Topics in Nutrition and Disease*; Spiller, G. A., Scala, J., Eds.; Alan R. Liss: New York, 1989; pp 109−228.
(17) Moriguchi, T.; Greiner, R. S.; Salem, N., Jr. *J. Neurochem.* **2000**, *75*, 2563−2573.
(18) Hamilton, J.; Greiner, R.; Salem, N., Jr.; Kim, H. Y. *Lipids* **2000**, *35*, 863−869.
(19) Tristram-Nagle, S.; Zhang, R.; Suter, R. M.; Worthington, C. R.; Sun, W. J.; Nagle, J. F. *Biophys. J.* **1993**, *64*, 1097−1109.

control unit. Absolute temperature readings were calibrated to a precision of ±0.5 °C.

^{1}H MAS NMR: The NOESY NMR experiments with magic angle spinning were conducted on a Bruker DMX500 widebore spectrometer at a resonance frequency of 500.13 MHz at a MAS spinning frequency of 10.00 or 10.25 kHz using a Bruker triple resonance MAS probe with double gas bearings for 4-mm rotors. Two-dimensional NOESY was carried out in the phase-sensitive mode.[20,21] The pulse sequence (d_1- 90° − t_1 − 90° − τ_m − 90° − acquire [t_2])$_n$ was employed: d_1 = 6 or 15 s; 512 t_1 increments; a 3.7-μs 90° pulse; mixing times, τ_m, from 5 to 800 ms; 2048 t_2 points; 16 scans per t_1-increment; and 3.3 kHz spectral width; a squared sine-bell window function was applied in both dimensions before 2D-Fourier analysis. Some cross-peaks of 18:0(d$_{35}$)-22:6n3PC had weak contributions from J-couplings that oscillated with the mixing time, τ_m. We suppressed these contributions with an additional π-pulse located at random positions within the mixing time period.[22] The position of the π-pulse was shifted with each t_1-increment. This altered the phase of J-cross-peaks at random, resulting in their cancellation. The magnetic field strength was locked to the internal D_2O resonance of the sample using the third channel of the MAS probe. The volumes of cross- and diagonal peaks in the two-dimensional spectra were determined by integration, and the relaxation rate matrix calculated as described previously.[23]

^{13}C MAS NMR: The experiments were carried out at 30±2 °C on Bruker DMX500 and DMX300 spectrometers at resonance frequencies of 125 and 75 MHz, respectively. The spin−lattice relaxation times, T_1, were measured at a MAS spinning frequency of 10 kHz by the inversion−recovery pulse sequence (d_1-180°-τ-90°-acquire), a delay time d_1= 11.5 s, a 5.5-μs 90° pulse, and a spectral width of 27.7 kHz. The experiments were conducted with 50 kHz of proton noise decoupling during data acquisition. The nuclear Overhauser enhancement was retained by application of 2 kHz of proton-noise decoupling starting 3 s before the application of ^{13}C pulses. Spectra were processed using a sine-bell window function before Fourier transformation. The baseline was corrected using a polynomial function of fifth order. The signal intensities were fitted to the equation $M(\tau) = M(0)(1-2\exp(-\tau/T_1))$ with $M(0)$ and T_1 as fit parameters.

The ^{13}C NMR cross-polarization experiments were conducted at a MAS spinning frequency of 5 kHz using a shaped spin-lock pulse that increments the carbon spin-lock field strength from 20 kHz to 25 kHz in 10 steps.[24] The spin-lock field strength for ^{1}H resonances was adjusted to achieve maximum signal intensity using an adamantane sample. Signal intensity of lipid samples was recorded as a function of contact time over the range from 100 μs to 300 ms. Application of the decoupling- and spin-lock fields increased the sample temperature by about 5±2 °C, as determined by conducting experiments at the gel-fluid phase transition of 1,2-dimyristoyl-sn-glycero-3-phosphocholine at 24 °C. The temperature calibration was corrected accordingly. The intensity of the ^{13}C magnetization as a function of contact time t, $M(t)$, was approximated by the following formula[25,26]

$$M(t) = M(0)\lambda^{-1}[1 - \exp(-\lambda t/T_{CH})]\exp(-t/T_{1\rho}(^1\mathrm{H})) \quad (1)$$

$$\lambda = 1 + (T_{CH}/T_{1\rho}(^{13}\mathrm{C})) - (T_{CH}/T_{1\rho}(^1\mathrm{H})) \quad (2)$$

where T_{CH} is the time constant of magnetization transfer from the ^{1}H spin reservoir to the ^{13}C reservoir and $T_{1\rho}(^1\mathrm{H})$ and $T_{1\rho}(^{13}\mathrm{C})$ are the rotating frame spin−lattice relaxation times of ^{1}H and ^{13}C, respectively. To improve precision of data analysis, the relaxation times, $T_{1\rho}(^{13}\mathrm{C})$, were measured by a pulse sequence similar to the cross-polarization experiments but without application of the spin-lock pulse for protons. The data were fitted to the function $M(t) = M(0)\exp(-t/T_{1\rho}(^{13}\mathrm{C}))$, where t is the length of the ^{13}C spin-lock pulse.

The signal intensity of resonances in the cross-polarization experiment were well described by eqs 1 and 2 (see Figure 12). The parameters $M(0)$, T_{CH}, and $T_{1\rho}(^1\mathrm{H})$ were determined using the nonlinear regression feature in Sigmaplot 8.0 (SPSS, Inc., Chicago, IL) that is based on the Levenberg−Marquardt algorithm. The rates of magnetization transfer from protons to carbons were of the order of milliseconds for DHA resonances near the carbonyl group and dozens of milliseconds for resonances near the terminal methyl group indicating differences in the strength of effective dipolar interactions along the polyunsaturated hydrocarbon chains. Using the measured/fitted values of $M(0)$, T_{CH}, $T_{1\rho}(^{13}C)$, and $T_{1\rho}(^1\mathrm{H})$, we established that signal intensity of ^{13}C resonances increases linearly up to 20% of the value of $M(0)$ to a very good approximation. The intensity in this range is solely determined by T_{CH} and $M(0)$. Consequently, we focused on measurements of peak intensities at short contact times to determine the T_{CH} values with high precision. Because of the strong variation in T_{CH} values, those contact times ranged from a fraction of a millisecond up to several milliseconds, depending on the particular carbon resonance. The intensity of partially superimposed resonances was determined by deconvolution using the deconvolution routine in XWINNMR 3.1 (Bruker Biospin Corp., Billerica, MA). Experimental errors of T_{CH} (approximately 10% in our experiments) depend solely on the signal-to-noise ratio of resonances.

X-ray Data Collection: Oriented Samples. The sample was mounted with the cylinder axis horizontal so that lamellar diffraction was along the vertical z-axis. X-rays of wavelength $\lambda = 1.2727$ Å with 1.5% energy dispersion were provided at the D1 line at CHESS (Cornell High Energy Synchrotron Source) from a monochromator consisting of two multilayers of W/B$_4$C (Osmic, Auburn Hills, MI). The multilayers were detuned slightly to minimize $\lambda/2$ radiation. Angular resolution in q_r of 0.001 Å^{-1} was achieved with slits. We varied the X-ray exposure times from 0.5 s to measure the lowest two orders, to 120 s to measure the diffuse scattering. For the longer time, the ratio of absorbed photons to the number of lipid molecules was less than 10^{-4} with a total flux on the sample of 6×10^9 photons/s. The diffraction data were collected using a CCD detector with 2048 × 2048 pixels and a pixel size of 40 μm.[27] We corrected the CCD data for distortion, intensity, zingers and dark count following the protocol of Barna et al.[28] and the files supplied by CHESS. The sample temperature (24.0 ± 0.2 °C) was controlled with a Neslab (Portsmouth, NH) controller and was measured with a NIST-calibrated Yellow Springs Instruments (Yellow Springs, Ohio) surface probe.

Capillary Samples. The X-ray source for these samples was a Rigaku fixed tube Cu source operated at 2.3 kW with a graphite monochromator to eliminate K_β radiation, yielding $\lambda = 1.5418$ Å. Three sets of Huber slits produced an in-plane resolution of 0.02 Å^{-1}. Experiments were conducted at 30 ± 0.2°C. Temperature was controlled by a Lake Shore Cryotronics Model DRC-91C temperature controller (Westerville, Ohio), which responded to a 1000-ohm platinum resistance thermometer (Rosemount, Minneapolis, MN) in the center of the sample chamber.

X-ray Analysis: The background was subtracted from X-ray scattering data of fully hydrated, oriented samples using scattering from regions well outside the region where diffuse lipid scattering occurred (between green lines and white areas in Figure 1.) A quadratic function was fitted to the background and the interpolated background was

(20) Jeener, J.; Meier, B. H.; Bachmann, P.; Ernst, R. R. *J. Chem. Phys.* **1979**, *71*, 4546−4553.
(21) Wagner, G.; Wuthrich, K. *J. Mol. Biol.* **1982**, *155*, 347−366.
(22) Macura, S.; Huang, Y.; Suter, D.; Ernst, R. R. *J. Magn. Reson.* **1981**, *43*, 259−281.
(23) Huster, D.; Arnold, K.; Gawrisch, K. *J. Phys. Chem. B* **1999**, *103*, 243−251.
(24) Metz, G.; Wu, X. L.; Smith, S. O. *J. Magn. Reson. A* **1994**, *110*, 219−227.
(25) Voelkel, R. *Angew. Chem., Int. Ed. Engl.* **1988**, *27*, 1468−1483.
(26) Michel, D.; Engelke, F. In *NMR Basic Principles and Progress*; Blumich, B., Ed.; Springer-Verlag: New York, 1994; pp 71−125.
(27) Tate, M. W.; Eikenberry, E. F.; Barna, S. L.; Wall, M. E.; Lowrance, J. L.; Gruner, S. M. *J. Appl. Cryst.* **1995**, *28*, 196−205.
(28) Barna, S. L.; Tate, M. W.; Gruner, S. M.; Eikenberry, E. F. *Rev. Sci. Instr.* **1999**, *70*, 2927−2934.

subtracted from the lipid scattering in the region delimited by the green box in Figure 1. The corrected intensity data were then analyzed as

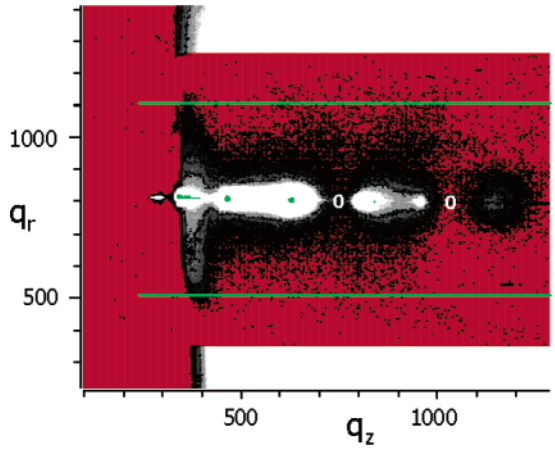

Figure 1. X-ray scattering data from 18:0(d_{35})-22:6n3PC as a function of pixel numbers in the q_z and q_r directions. The small, light region near q_z = 300 pixels is the attenuated beam, the intense scattering in the region q_z = 350 pixels is reflectivity, mostly from the mica, which is strongly attenuated for larger q_z but is still significant for q_r near 0 which is located near 820 pixels. The green dots near q_z = 460 and 640 are the first two orders of diffraction which are saturated in this 120 s exposure. At less than saturation, intensity is strongest in the white pixels. The red pixels indicate an intensity value of 10 or less. Zeroes in the form factor (indicated) occur near qz = 750 and 1030 pixels.

previously described.[29] The measured intensity $I(q)$ is the product, $I(q) = S(q)|F(q_z)|^2 \mathrm{Abs}(q_z)/q_z$ of a structure factor $S(q)$ and a form factor $F(q_z)$ squared, as well as the usual q_z^{-1} Lorentz factor for oriented cylindrical samples and an absorption factor $\mathrm{Abs}(q_z)$,[30,31] which was calculated using the absorbance decay length of 2.2 mm for lipid/water mixtures for the wavelength of X-rays used. The structure factor depends primarily on the bulk modulus for layer compression, B, and the bending modulus of monolayers, k_c.[29,32] Analysis of the q_r dependence yielded k_c values in the range $1.1-1.2 \times 10^{-12}$ ergs for both lipids, and values for B of 1.3×10^{12} ergs/cm^4 for 18:0(d_{35})-22:6n3PC and 2.5×10^{12} ergs/cm^4 for 18:0(d_{35})-22:5n6PC. Within these ranges the form factors obtained from eq 1 were only modestly affected by values of B and k_c used to calculate $S(q)$. For smaller q_z, corresponding to the first and second orders, domain size also affects $S(q)$. Domain sizes L_r and L_z were estimated from q_z near the first and second diffraction orders to be 30 μm and 0.2 μm, respectively. It was found that the form factors were not much affected by substantial variations in L_r and L_z when diffuse intensities were used that had q_r values at least 50 pixels away from $q_r = 0$. The final $F(q_z)$ was then obtained from $S(q)$ and the measured $I(q)$ taken from $50 < q_r < 65$ pixels. $F(q_h)$ was then read at the Bragg orders, q_h for $h = 2-6$. The sharp first two orders observed at short exposure times gave $D = 66.2 \pm 0.2$ Å for 18:0(d_{35})-22:6n3PC, and $D = 65.2 \pm 0.2$ Å for 18:0(d_{35})-22:5n6PC; the ratio of the intensities of these first two orders also provides estimates for $F(q_1)$ which is not well determined by the diffuse scattering method.[29] The value of $F(0)$ was determined[33] using $F(0) = 2(n_L - V_L \rho_W)/A$, where $n_L = 458$ is the number of electrons in 18:0(d_{35})-22:6n3PC, $n_L = 460$ is the number of electrons in 18:0(d_{35})-22:5n6PC, V_L is the molecular volume, 1359 $\pm$ 3 Å^3 for 18:0(d_{35})-22:6n3PC and 1366$\pm$3 Å^3 for 18:0(d_{35})-22:5n6PC, $\rho_w = 0.333$e/Å^3 is the electron density of water at 30 °C. $F(0)$ is calculated to be 0.16 e/ Å^2 for 18:0(d_{35})-22:6n3PC and 0.19 e/ Å^2 for 18:0(d_{35})-22:5n6PC, and A is the area/lipid (calculated below). Molecular volume measurements were carried out as in Wiener et al.[34] Relative electron density profiles were then obtained by Fourier reconstruction, $\rho_z = K\sum_{h=0}^{h=6} F_h \cos(2\pi hz/D)$, where K is the instrumental scaling factor. The phases (- -++- -) of F_h were obvious from the zeroes in the data shown in Figure 1. The relative continuous transform (Figure 14) was calculated using the Shannon sampling theorem.[35] The form factors at less than full hydration were obtained by integrating the intensity of the Bragg orders; no correction was made for fluctuations.

Area Calculation: The area/lipid A_L is obtained[36-39] by comparing the data to the recently published, well-determined structure of gel phase DMPC as a reference state.[40] Care was taken to compare to a gel phase DMPC profile constructed from six orders of diffraction, which has the same q_z range as the fluid phase data.

Molecular Dynamics Simulations: The simulation protocol employed has been successfully applied to the simulation of saturated, unsaturated, and polyunsaturated phosphatidylcholine bilayers in the recent past[41-44] and is described here for completeness. The periodic simulation cell contained 72 lipids (36 per monolayer) and 15.1 water molecules/lipid. A partially flexible simulation cell was employed with the z dimension (i.e., the bilayer normal) adjusted to maintain the P_{zz} = 1 atm, and the x and y dimensions fixed to maintain a surface area of 67.2 Å^2/molecule, as estimated from previous X-ray diffraction experiments on SDPC at this water content.[45] Initial coordinates of the DHA chain were generated by carrying out Langevin dynamics simulations of a single molecule and then combining randomly selected conformations onto lipids from a previous simulation of 1-palmitoyl-2-oleoyl-sn-glycero-3-phosphocholine.[44] The stearoyl chain conformations were generated by placing two additional carbon atoms (in the trans conformation) at the end of the palmitic acid. The DPA lipid bilayer was generated from the DHA bilayer simulation by converting the last double bond to a single bond.

The program CHARMM (Chemistry at HARvard Molecular Mechanics[46,47] was used with the PARM22b4b all-atom parameter set[48,49] and its extension to polyunsaturated lipids.[43] The CHARMM potential contains internal energy terms for bond lengths, bond angles, torsional angles, and improper torsional angles. The interactions between nonbonded atoms are described by Coulombic interactions between partial point charges on the atomic centers and a Lennard−Jones (LJ) 6−12 potential. The LJ potential was switched smoothly to zero over the region from 10 to 12 Å. Electrostatic interactions were included

(29) Lyatskaya, Y.; Liu, Y. F.; Tristram-Nagle, S.; Katsaras, J.; Nagle, J. F. *Phys. Rev. E* **2001**, *6301*, 011907.
(30) Wiener, M. C.; White, S. H. *Biophys. J.* **1991**, *59*, 162−173.
(31) Wiener, M. C.; White, S. H. *Biophys. J.* **1991**, *59*, 174−185.
(32) Zhang, R. T.; Suter, R. M.; Nagle, J. F. *Phys. Rev. E* **1994**, *50*, 5047−5060.
(33) Nagle, J. F.; Wiener, M. C. *Biophys. J.* **1989**, *55*, 309−313.
(34) Wiener, M. C.; Tristram-Nagle, S.; Wilkinson, D. A.; Campbell, L. E.; Nagle, J. F. *Biochim. Biophys. Acta* **1988**, *938*, 135−142.
(35) Worthington, C. R.; King, G. I.; Mcintosh, T. J. *Biophys. J.* **1973**, *13*, 480−494.
(36) Nagle, J. F.; Tristram-Nagle, S. *Biochim. Biophys. Acta* **2000**, *1469*, 159−195.
(37) Nagle, J. F.; Tristram-Nagle, S. *Curr. Opin. Struct.Biol.* **2000**, *10*, 474−480.
(38) Mcintosh, T. J.; Simon, S. A. *Biochemistry* **1986**, *25*, 4948−4952.
(39) Mcintosh, T. J.; Simon, S. A. *Biochemistry* **1986**, *25*, 4058−4066.
(40) Tristram-Nagle, S.; Liu, Y.; Legleiter, J.; Nagle, J. F. *Biophys. J.* **2002**, *83*, 3324−3335.
(41) Feller, S. E.; MacKerell, A. D., Jr. *J. Phys. Chem. B* **2000**, *104*, 7510−7515.
(42) Feller, S. E.; Huster, D.; Gawrisch, K. *J. Am. Chem. Soc.* **1999**, *121*, 8963−8964.
(43) Feller, S. E.; Gawrisch, K.; MacKerell, A. D. *J. Am. Chem. Soc.* **2002**, *124*, 318−326.
(44) Armen, R. S.; Uitto, O. D.; Feller, S. E. *Biophys. J.* **1998**, *75*, 734−744.
(45) Koenig, B. W.; Strey, H. H.; Gawrisch, K. *Biophys. J.* **1997**, *73*, 1954−1966.
(46) Brooks, B. R.; Bruccoleri, R. E.; Olafson, B. D.; States, D. J.; Swaminathan, S.; Karplus, M. *J. Comput. Chem.* **1983**, *4*, 187−217.
(47) MacKerell, A. D., Jr.; Brooks, B.; Brooks, C. L. I.; Nilsson, L.; Roux, B.; Won, Y.; Karplus, M. C. In *Encyclopedia of Computational Chemistry*; Schleyer, P. v. R., Allinger, N. L., Clark, T., Gasteiger, J., Kollman, P. A., Schaefer, H. F. I., Schreiner, P. R., Eds.; John Wiley & Sons: Chichester, 1998; pp 271−277.
(48) Schlenkrich, M.; Brickmann, J.; MacKerell, A. D., Jr.; Karplus, M. In *Biological Membranes: A Molecular Perspective from Computation and Experiment*; Merz, K. M., Roux, B., Eds.; Birkhäuser: Boston, 1996; pp 31−81.
(49) Feller, S. E.; Yin, D. X.; Pastor, R. W.; MacKerell, A. D. *Biophys. J.* **1997**, *73*, 2269−2279.

via the particle mesh Ewald summation.[50] All covalent bonds involving hydrogen were fixed at their equilibrium distances using the SHAKE algorithm.[51] A time step of 2 fs was employed with a leapfrog Verlet integration scheme. A neighbor list, used for calculating the LJ potential and the real space portion of the Ewald sum, was kept to 12 Å and updated every 20 fs. A variant of the extended system formalism, the Langevin Piston algorithm,[52] was used to control the normal pressure. The temperature was maintained at 30 °C by means of a Hoover thermostat.[53] Coordinate sets were saved every 1 ps for subsequent analysis. Simulations were carried out using eight processors on a Beowulf-type parallel computer, with each nanosecond of simulation taking approximately 5 days of wall time. The total length of each simulation was 16 ns, with the first nanosecond discarded as equilibration.

Results

Phase Behavior. The ^{31}P NMR spectra (Supporting Information) and the ^{2}H NMR spectra of both lipids at temperatures below −2.5 °C are characteristic of a lamellar gel phase (spectrum not shown) and above −2.5 °C of a lamellar fluid phase (Figure 2). No other phase transitions were detected over

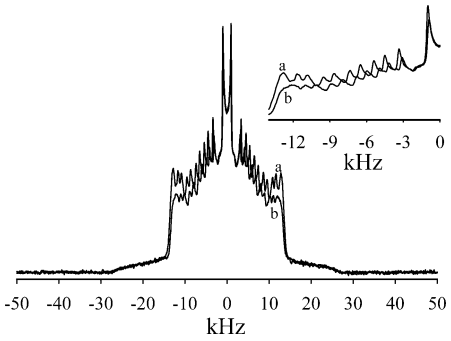

Figure 2. ^{2}H NMR spectra of (a) 18:0(d_{35})-22:5n6PC and (b) 18:0(d_{35})-22:6n3PC at 25 °C in 50 wt % deuterium depleted water. The inset shows the expanded central section of the spectra. Stearic acid chain order parameters are lower in 18:0(d_{35})-22:6n3PC.

the range from −20 to +70 °C. The first moments, M_1, of the ^{2}H NMR spectra were calculated according to the formula[54] $M_1 = \int_0^\infty \omega f(\omega) d\omega / \int_0^\infty f(\omega) d\omega$, where $f(\omega)$ is the intensity of the NMR spectrum as a function of the frequency offset ω ($\omega = 0$ corresponds to the Larmor frequency of the ^{2}H nucleus). The accurate gel-fluid phase transition temperature was obtained by plotting the first moment of the ^{2}H NMR spectra recorded at temperature intervals of 1 °C from low to high temperature[55] (Figure 3). The loss of a double bond from DHA to DPA had no influence on the main phase transition temperature. Upon cooling, both lipids had a hysteresis of the main phase transition of 10−15 °C to lower temperature (data not shown).

^{2}H NMR Order Parameter Profiles. Spectra were dePaked[56] and smoothed order parameter profiles calculated as described previously.[55] As compared to 18:0(d_{35})-22:6n3PC, the order parameters of perdeuterated stearic acid in 18:0(d_{35})-22:5n6PC

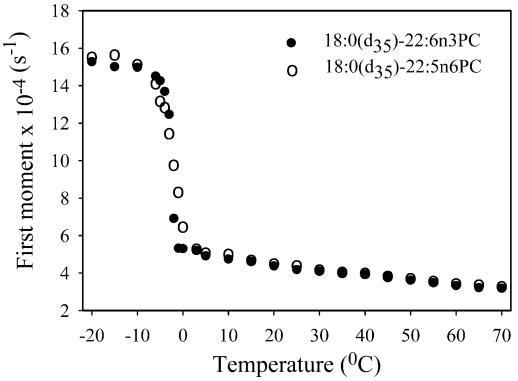

Figure 3. First moments of the ^{2}H NMR spectra of the perdeuterated sn-1 chains of 18:0(d_{35})-22:6n3PC (●) and 18:0(d_{35})-22:5n6PC (○) plotted as a function of temperature. Experiments were conducted from low to high temperature. Both lipids have the same gel-fluid phase transition temperature of −2.5 °C.

are slightly higher for the methylene segments near the carbonyl group (plateau region) and significantly higher in the middle of the chain near carbon atoms C_{10-12} (see Figure 4). Order

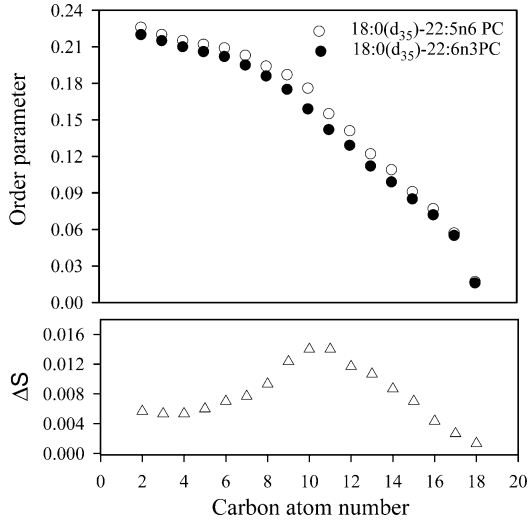

Figure 4. The sn-1 chain order parameter profiles of 18:0(d_{35})-22:6n3PC (●) and 18:0(d_{35})-22:5n6PC (○) at 25 °C. The bottom part shows the difference in sn-1 order between both lipids. Stearic acid chain order is significantly lower in 18:0(d_{35})-22:6n3PC, in particular for chain segments that are located in the center of the bilayer.

parameters in the fluid phase decrease with increasing temperature, but the difference in sn-1 chain order between both lipids shows little temperature dependence. The slightly larger sn-1 chain order parameters for 18:0(d_{35})-22:5n6PC could be interpreted as arising from a somewhat smaller area per lipid molecule. However, according to the X-ray studies (vide infra) there is no statistically significant difference in area per molecule between the lipids. Furthermore, the change in average order parameter ($\Delta S = +0.008$) is reproduced in the MD simulations ($\Delta S = +0.007$) that were carried out with identical areas per molecule. The lesson is that area per molecule and hydrophobic thickness of bilayers composed of mixed-chain polyunsaturated lipids cannot be determined accurately from sn-1 chain order parameters only. We conclude that the ^{2}H NMR experiment is probing changes in sn-1 chain structure that are caused by the removal of the double bond from the polyunsaturated chain in position sn-2.

(50) Darden, T.; York, D.; Pedersen, L. *J. Chem. Phys.* **1993**, *98*, 10 089−10 092.
(51) Ryckaert, J. P.; Ciccotti, G.; Berendsen, H. J. C. *J. Comput. Phys.* **1977**, *23*, 327−341.
(52) Feller, S. E.; Zhang, Y. H.; Pastor, R. W.; Brooks, B. R. *J. Chem. Phys.* **1995**, *103*, 4613−4621.
(53) Hoover, W. G. *Phys. Rev. A* **1985**, *31*, 1695−1697.
(54) Davis, J. H. *Biochim. Biophys. Acta* **1983**, *737*, 117−171.
(55) Holte, L. L.; Peter, S. A.; Sinnwell, T. M.; Gawrisch, K. *Biophys. J.* **1995**, *68*, 2396−2403.
(56) Sternin, E.; Bloom, M.; Mackay, A. L. *J. Magn. Reson.* **1983**, *55*, 274−282.

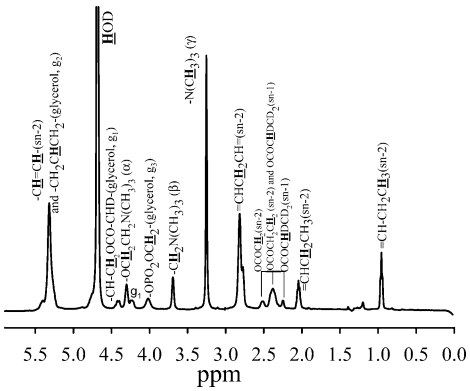

Figure 5. ^{1}H MAS NMR spectrum of 18:0(d_{35})-22:6n3PC in D_2O (50 wt %) with signal assignments.

^{1}H MAS NOESY Relaxation Rates. Excellent resolution of the ^{1}H NMR resonances was achieved with both polyunsaturated lipids, particularly those resonances near the terminal methyl end. The line width at half-height varied from 25 Hz for the glycerol resonances to 3 Hz for the proton resonances arising from carbons C_{21} and C_{22} of the polyunsaturated DHA chain, allowing resolution of the J-coupling of 7 Hz. The ^{1}H MAS NMR spectrum of 18:0(d_{35})-22:6n3PC is shown in Figure 5 along with the signal assignment. The intensity of NOESY cross-peaks (Figure 6) reaches a maximum at mixing times

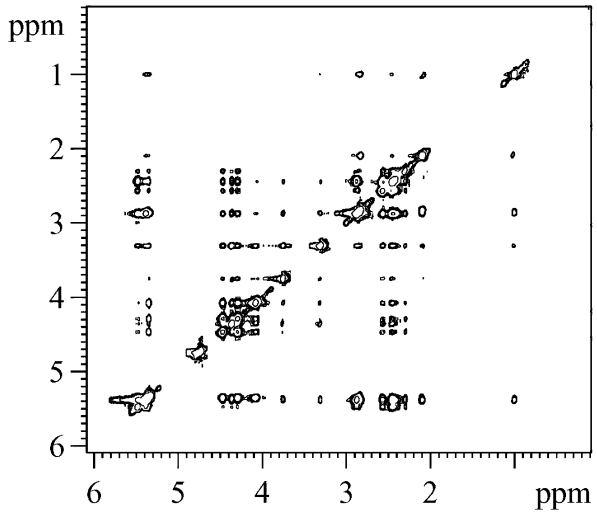

Figure 6. NOESY spectrum of 18:0(d_{35})-22:6n3PC recorded at a mixing time of 300 ms. The intensity of cross-peaks varies significantly from resonance to resonance, indicating differences in the probability of contact between the corresponding protons as well as differences in motional correlation times.

between 300 and 500 ms, decreasing at longer mixing times due to spin−lattice relaxation. Similar behavior has been observed for other lipids.[23,57] Spin−lattice and cross-relaxation rates were calculated as described in Materials and Methods.

The spin−lattice relaxation rates of DHA and DPA agree within experimental error, with the exception of the terminal methyl group of the polyunsaturated chains where the DPA result is higher by a factor of 1.5. The cross-relaxation rates from the choline methyl resonance to all other resonances are reported in Figure 7. As expected from their average location along the bilayer normal, the rates of magnetization transfer to

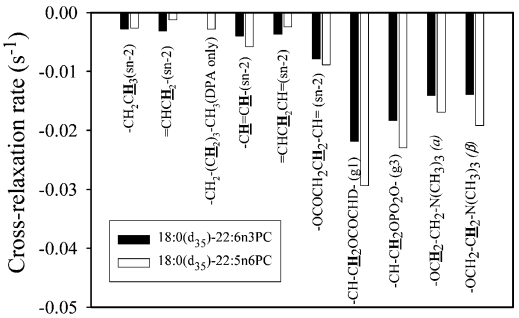

Figure 7. Cross-relaxation rates of magnetization transfer from the headgroup choline protons (γ) to all other resolved proton resonances recorded at 25 °C of 18:0(d_{35})-22:6n3PC (black bars) and 18:0(d_{35})-22:5n6PC (white bars). Magnetization transfer to lipid segments residing at the same depth in the bilayer is strongest. However, nonnegligible rates are observed to almost all other segments highlighting the structural disorder of lipids in fluid bilayers.

the headgroup region, the glycerol group, and to protons of upper chain segments are high, whereas cross-relaxation rates to lipid resonances from hydrocarbon chains at the center of the bilayer are more than 1 order of magnitude lower. Although the cross-relaxation rates between very distant groups, e.g., the choline resonances and the resonances at the methyl end of polyunsaturated hydrocarbon chains, are small, they are observed in our experiments. In this regard, polyunsaturated lipids are not unique.

In experiments on saturated lipids, we established earlier that such seemingly unusual transfers are the result of a low, but finite, probability of direct intermolecular contact between these, on average, distant protons rather than the result of spin-diffusion.[23,57] The efficiency of spin diffusion along lipids in the fluid phase is very low because of rapid conformational transitions that average out the dipolar interactions between neighbored lipid segments. Although the polyunsaturated chains have fewer degrees of freedom, the energy barrier for rotation about the C−C bonds of the methylene groups between double bonds (less than 1 kcal mol^{-1}) is much lower than the rotational barriers in saturated chains (more than 3 kcal mol^{-1}).[43] These low rotational barriers allow for rapid conformational transitions in polyunsaturated chains, producing a high degree of conformational disorder and allowing cross-relaxation between headgroup and chain resonances. Everts and Davis[58] observed similar magnetization transfer between the methylene segments of DHA and choline using a ^{1}H−^{13}C cross-polarization experiment, but did not detect similar interactions between the choline group and the stearic acid chain. The NOESY experiments on 18:0−22:6n3PC with a protonated stearic acid chain (results not shown) detected both choline to DHA as well as choline to stearic acid magnetization transfer at rates that are identical within experimental error.

The differences between cross-relaxation rates of choline to DHA or DPA chain resonances are smaller than the experimental error of the measurements. These rates are a function of both membrane structure (proton−proton distances and orientations) and dynamics (the correlation time of the internuclear vector). To ensure that the agreement between DHA and DPA results was not a fortuitous cancellation of these two effects, we calculated the correlation function for the proton−proton dipolar interaction, $C(t)$, from the MD simulation

(57) Huster, D.; Gawrisch, K. *J. Am. Chem. Soc.* **1999**, *121*, 1992−1993.

(58) Everts, S.; Davis, J. H. *Biophys. J.* **2000**, *79*, 885−897.

trajectories using methods we have described previously.[42] Figure 8 shows the calculated correlation function of dipolar

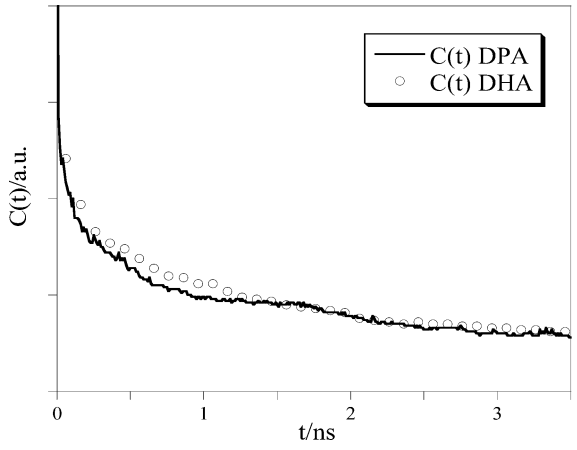

Figure 8. Correlation functions of proton−proton dipolar interactions between the choline headgroup and the methylene group C_{21} of the polyunsaturated chains in 18:0−22:6n3PC and 18:0:22:5n6PC. Within statistical error the effective strength of dipolar interaction is the same for both polyunsaturated chains.

interactions between the choline methyl protons and the C_{21} methylene protons of the DHA and DPA chains. Both the probability of contact, which is proportional to the intensity of the correlation function at $t = 0$, and the decay time for the correlation function, are comparable for the two lipids, confirming that both DHA- and DPA-containing membranes are disordered to roughly the same extent.

^{13}C MAS NMR. Assignment of Olefin Resonances. The resolution of ^{13}C resonances for both lipids was excellent, especially in the olefin region of the spectrum, where only two of the twelve DHA- and the ten DPA-resonances are superimposed. The ^{13}C spectrum of 18:0(d_{35})-22:6n3PC is shown in Figure 9, along with the signal assignment of olefin carbons.

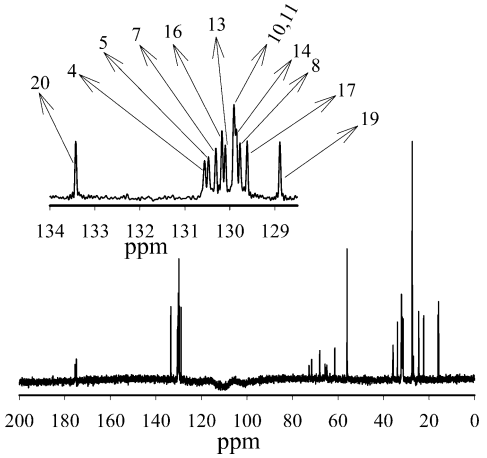

Figure 9. ^{13}C MAS NMR spectrum of 18:0(d_{35})-22:6n-3PC in 50 wt % D_2O with signal assignments of olefin carbons. Ten out of twelve olefin resonances are fully resolved.

Initial assignment was based on the assumption that spin−lattice relaxation times increase steadily from the glycerol group to the terminal methyl group as found in the simulations. This assignment is consistent with the limited information available from other measurements and from published results: the chemical shift of the carbon C_4 agreed with the chemical shift

Table 1. ^{13}C Spin−Lattice Relaxation Times, T_1, and the Cross-Polarization Time Constants[a], T_{CH}, of Carbons of DHA and DPA in 18:0(d_{35})-22:6n3PC and 18:0(d_{35})-22:5n6PC, Respectively, Recorded at a Resonance Frequency of 125.7 MHz and a Temperature of 30 ± 2 °C

chemical shift (ppm)	chemical shift (ppm)		T_1 (^{13}C) (s)		T_{CH} (ms)	
DHA	DPA	assignment	DHA	DPA	DHA	DPA
35.82	35.82	C2	0.34	0.28	1.26	1.514
24.48	24.50[b]	C3	0.36	- -[b]	0.914	- -[b]
130.63	130.65	C4	0.52	0.51	2.55	2.05
130.54	130.47	C5	0.53	0.44	3.77	3.95
130.30	130.38	C7	0.78	0.89	4.28	3.00
129.76	129.92	C8	0.83	1.00	16.00	7.17
129.90	129.77	C10,C11	1.10	0.97	7.30	3.20
130.10	130.12	C13	1.15	1.18	3.73	3.74
129.85	130.17	C14	1.43	1.25	20.00	21.00
130.17	129.55	C16	1.92	1.46	36.00	12.00
129.60	131.79	C17	1.98	1.44	16.00	19.00
- - -	29.09	C18	- -	1.08	- -	4.60
128.89	31.35	C19	3.13	1.22	38.00	3.090
133.44	33.48	C20	3.40	1.56	33.00	3.730
22.42	24.50[b]	C21	3.85	- -[b]	23.00	- -[b]
15.99	15.85	C22	4.22	3.17	24.00	19.00

[a] measured at a spinning frequency of 5 kHz. [b] The C_3 and C_{21} carbon signals are superimposed in the ^{13}C spectrum of 18:0(d_{35})-22:5n6PC; The time constant of magnetization transfer was determined from the rise of signal amplitudes at the commencement of the C−H contact.

of C_4 in ^{13}C labeled DHA that was incorporated as free fatty acid at low concentration into a matrix of 1-stearoyl-2 docosahexaenoyl-sn-glycero-3-phosphocholine. This resonance was assigned with a ^{13}C−^{13}C COSY experiment on the free fatty acid (results not shown). The assignment of DHA resonances for carbons C_{20}, C_{19}, and C_{17} agrees with values that have been reported in the literature.[59] The resonances C_{10} and C_{11} in the center of the chain are superimposed. Signal assignments and spin−lattice relaxation times are reported in Table 1, and Figure 9,11.

The relaxation times were observed to increase in a stepwise fashion from double bond to double bond toward the terminal methyl end (see Table 1, Figure 11). The spin−lattice relaxation rates, $1/T_1$, depend on the spectral density function $J(\omega)$ according to

$$\frac{1}{nT_1} = \frac{1}{10}\left(\gamma_C\gamma_H\frac{h}{2\pi}\frac{1}{r_{CH}^3}\right)^2 \times (J(\omega_C - \omega_H) + 3J(\omega_C) + 6J(\omega_C + \omega_H)) \quad (3)$$

where n is the number of protons per carbon, γ_H, and γ_C's are the magnetogyric ratios for protons and carbons respectively, h is Planck's constant, and ω_C and ω_H are the resonance frequencies of carbons and protons, respectively. The connection between the correlation functions of chain motions, $C(t)$, and the experimentally measured spin−lattice relaxation rates is through the spectral density function (the Fourier transform of the correlation function)

$$J(\omega) = \int_0^\infty C(t)\cos(\omega t)dt \quad (4)$$

Considering a simple exponential decay of $C(t)$ we obtain the following dependence of spectral density on motional correlation time τ

(59) Batchelor, J. G.; Cushley, R. J.; Prestegard, J. H. *J. Org. Chem.* **1974**, *39*, 1698−1705.

$$C(t) = C(0)e^{-t/\tau} \rightarrow J(\omega) = \frac{2C(0)\tau}{1 + \tau^2\omega^2} \qquad (5)$$

The ^{13}C spin−lattice relaxation rates, $1/T_1$, were also calculated from the simulation trajectory for both DHA and DPA containing lipids. The starting point for such a calculation is the second rank reorientational correlation function

$$C(t) = \langle P_2(\bar{\mu}(0) \bullet \bar{\mu}(t)) \rangle \qquad (6)$$

where P_2 is the second-order Legendre polynomial and $\bar{\mu}(t)$ is the unit vector directed along the C−H bond at time t. The brackets in eq 6 represent an averaging over all lipids and over all time intervals.

The simulations revealed a dramatic difference in chain dynamics between the saturated stearic acid and the polyunsaturated docosahexaenoic acid at carbon C_{12} (data not shown). The stearic acid correlation functions had a lower decay rate and reached a constant value different from zero at times longer than 5 ns. The correlation function of C_{12} of DHA decayed more rapidly, reaching zero within 2 ns. The faster decay for DHA is indicative of more rapid motions, whereas the decay to zero indicates a very low order parameter of the corresponding C−H bond.

Furthermore, we observed a strong gradient of motional correlation times along the polyunsaturated chains. To describe the relaxation of the reorientational correlation functions, from which the T_1 were calculated, the correlation function for each carbon position was fit to a sum of 4 exponentials, $C(t) = \sum_{i=1}^{4} a_i e^{-t/\tau_i}$. The data and the exponential fits are presented in Figure 10 for C_2 (upper panel) and C_{21} (lower panel) of the DHA chain. For each function the average decay time, $\tau_{ave} = \sum_{i=1}^{4} a_i\tau_i / \sum_{i=1}^{4} a_i$, was calculated to give a measure of the relaxation times. The differences in the correlation functions show clearly the dramatic difference in dynamics at the two ends of the chain with τ_{ave} values of 1.2 ns and 7 ps for C_2 and C_{21}, respectively. The nanosecond correlation times are typical for lipid rotation about their long axis as well as wobble of the entire lipid molecule.[42] In contrast, the motions near the methyl terminal end of DHA are dominated by internal chain isomerization.

According to eqs 3 and 5, motions with correlation times in the nanosecond range are most effective in enhancing spin−lattice relaxation, leading to shorter T_1-values. Furthermore, motional correlation times of nanoseconds or longer result in a T_1-dependence on magnetic field strength. Such a field dependence was observed for DHA and DPA resonances of chain segments near the carbonyl group, e.g. T_1 for carbons C_2 and C_3 of DHA decreased by 42% and 53%, respectively upon increase of the ^{13}C resonance frequency from 75.4 to 125.7 MHz. In contrast, relaxation times toward the terminal methyl group are significantly higher and any field dependence is smaller than the exerimental error. Therefore, the polyunsaturated chain segments near the terminal methyl group must be moving with correlation times in the picosecond range as predicted by the simulations. However, even at the methyl terminal end the slower motions are not entirely absent as seen from differences between $T_{1\rho}$(^{13}C) and T_1. The values of $T_{1\rho}$(^{13}C) vary from 0.02 ± 0.01 s at carbon C_4 to 0.14 ± 0.07 s at carbon C_{20} compared 0.52 ± 0.03 s and 3.4 ± 0.2 s for T_1, respectively. Although the experimental error of our $T_{1\rho}$(^{13}C) values is large (up to 50%), the $T_{1\rho}$(^{13}C) values are about 1 order of magnitude lower than T_1 (see also Everts and Davis[58]).

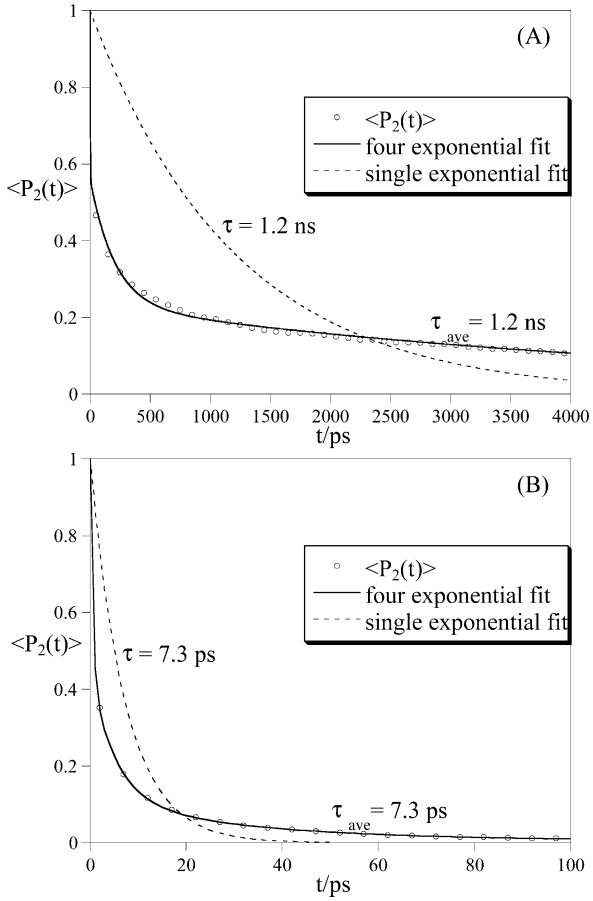

Figure 10. Correlation functions of proton-carbon dipolar interactions at carbon C_2 (upper panel) and carbon C_{21} (lower panel) of DHA in 18:0(d_{35})-22:6n3PC. The full line represents a fit to the calculated correlation function using superposition of four exponentials (see text for definitions). The correlation function at C_{21} decays orders of magnitude more rapidly, confirming that the methyl terminal end of DHA performs fast, large amplitude motions. Included in each panel is a plot of a simple exponential decay with a decay time equal to τ_{ave} (dashed line). A comparison of this curve with the actual correlation function data shows clearly the complex relaxation that is occurring on time scales from femtoseconds to multi-nanoseconds

The comparison of reorientational correlation functions of DHA and DPA reveals that for positions near the top of the chain, the decay is very similar, with relaxation times that become progressively shorter down the chain. The chain dynamics are distinctly different for DHA and DPA at the methyl end. Here the presence of an additional double bond imparts faster reorientational dynamics to the DHA segments, as seen in Figure 11. The difference in relaxation rates extends to the middle of the lipid chains. It can be understood in terms of the much higher isomerization rate observed for dihedral angles found between double bonds. As described by Feller, Gawrisch, and MacKerell,[43] the rotational barrier for methylene segments separating double bonds is extremely low (<1 kcal/mol) leading to high rates of chain isomerization. The loss of a double bond in DPA eliminates two C−C bonds with low barriers to rotation resulting in motional restrictions and longer correlation times at the terminal methyl end of DPA. Calculated and measured spin−lattice relaxation times are in good quantitative agreement, although there is a tendency for the differences between DHA and DPA near the terminal methyl to be

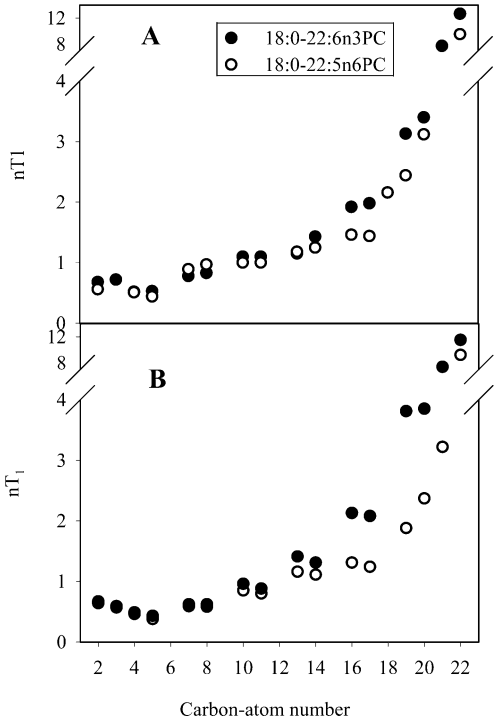

Figure 11. Measured (A) and calculated (B) spin lattice relaxation times, T_1. The relaxation times were multiplied by the number of directly bound protons per carbon to provide a better measure of chain dynamics. Note that relaxation times change by more than 1 order of magnitude from C_2 to C_{22}.

somewhat larger in the simulations. It could stem from weak contributions to relaxation other than dipolar interactions from directly bonded protons, and from absence of slower collective modes of motion in the simulations.

^{1}H-^{13}C Cross-Polarization. The rapid chain motions in the liquid crystalline state effectively suppress magnetization transfer between proton resonances by spin diffusion. Therefore, magnetization transfer from the protons to a particular carbon resonance at reasonably short contact times is dominated by a transfer from the directly bonded protons. This was confirmed in a ^{1}H-^{13}C cross-polarization experiment with selective presaturation of proton resonances conducted by Everts and Davis.[58] These authors suggested measuring cross-polarization growth curves for determination of the strength of residual dipolar couplings. We conducted such experiments on both polyunsaturated lipids (Figure 12, Table 1). The rate of magnetization transfer under spin-lock conditions, $1/T_{CH}$, is proportional to the spectral density function $J(\Delta\omega_C)$ of the cross-polarization process.[26] The functional dependence of $1/T_{CH}$ on chain motions can be evaluated by assuming that the r.f. fields for both carbons and protons are applied in resonance, matching the Hartmann−Hahn condition, giving $1/T_{CH} = 1.681\ M_2^{CH}/(M_2^{HH})^{1/2}$, where M_2^{CH} and M_2^{HH} are the van Vleck second moments of ^{1}H−^{13}C− and ^{1}H−^{1}H dipolar interactions, respectively.[26]

The M_2^{CH} and M_2^{HH} second moments are proportional to the square of the corresponding dipolar interactions between directly bonded carbons and protons as well as between neighbored protons, respectively. The effect of motions on dipolar interactions is conveniently described by a segmental order parameter. The effective strength of the ^{1}H−^{13}C− and ^{1}H−^{1}H dipolar interactions is linked by a proportionality factor that depends on bond geometry and the number of interacting protons per

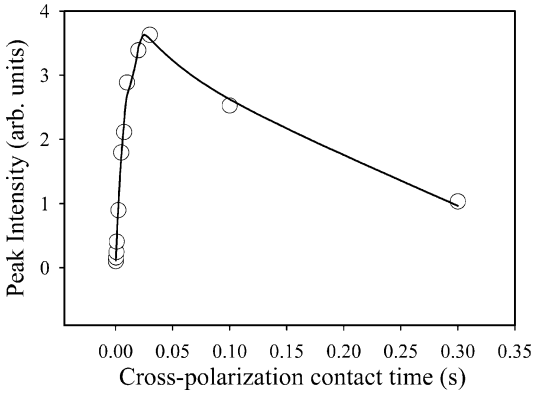

Figure 12. Intensity of the ^{13}C resonance of olefin carbon C_8 in the DHA chain of 18:0(d_{35})-22:6n3PC as a function of cross-polarization contact time. The initial rate of intensity increase is determined by the effective strength of dipolar interactions between protons and carbons expressed as cross-polarization time constant T_{CH}. Intensity decreases due to rotating frame spin−lattice relaxation of carbon and proton nuclei ($T_{1\rho}$(^{13}C) and $T_{1\rho}$(^{1}H)).

carbon. As a consequence, the rate of magnetization transfer, $1/T_{CH}$, is proportional to the bond order parameter S_{CH}. To report absolute values of order parameters for all resolved carbons, the values of $1/T_{CH}$ were calibrated separately to the measured ^{2}H NMR order parameters of methyl groups, methylene groups, and olefin carbons.

For the calibration we used partially assigned ^{2}H NMR order parameters from a previous experiment conducted on 18:0−22:6n3(d_{31})PC with a perdeuterated DHA chain.[60] The T_{CH} values of methyl groups were related to the measured ^{2}H NMR order parameter of the terminal methyl group of DHA ($S_{CD3} = 0.008$). The order parameters of methylene groups were related to the averaged order parameter ($S_{av} = 0.101$) of the two nonequivalent protons at C_2 of DHA ($S_{CD(1)} = 0.115$; $S_{CD(2)} = 0.088$). Order parameters of double bonds were calculated assuming that the C_4 of DHA has the highest order parameters of double bonds ($S_{CD} = 0.046$). The strength of quadrupolar interactions is higher than the strength of dipolar interactions by almost 1 order of magnitude. Therefore, the order parameters determined via the dipolar interactions are sensitive to somewhat slower collective motions in the lipid bilayer with correlation times from micro- to milliseconds. However, such motions reduce order parameters of all lipid segments by the same factor. Therefore, the calibration to the order parameters measured by ^{2}H NMR corrects for such differences.

The experimentally assigned order parameter profiles of DHA and DPA in 18:0(d_{35})-22:6n3PC and 18:0(d_{35})-22:5n6PC, respectively, are presented in Figure 13. The redundancy in order parameters determined by $1/T_{CH}$ values and ^{2}H NMR suggests that experimental errors of order parameters determined via T_{CH} measurements are of the order of 20%. This is reasonable, given the experimental error in T_{CH} and the approximations in the theory. Order parameters from ^{2}H NMR measurements on deuterated DHA chains were reported earlier,[43,60,61] however, they could not be experimentally assigned to specific carbon atoms. Additionally, the order parameter of the olefin carbon C_4 ($S = 0.05$) is by a factor of 1.6 lower than the value reported by Huber et al.[61] Although we are uncertain about the origin of

(60) Gawrisch, K.; Eldho, N. V.; Mathews, J. S.; Lindsay, C. C. *Biophys. J.* **2002**, *82*, 13.
(61) Huber, T.; Rajamoorthi, K.; Kurze, V. F.; Beyer, K.; Brown, M. F. *J. Am. Chem. Soc.* **2002**, *124*, 298−309.

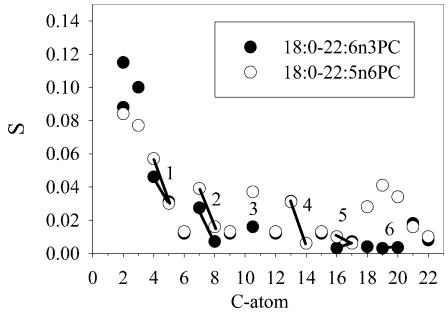

Figure 13. Order parameter profiles of DHA and DPA chains in 18:0(d_{35})-22:6n3PC (●) and 18:0(d_{35})-22:5n6 PC (○), respectively. Order parameters were determined from measurements of T_{CH} cross-polarization rates, calibrated to ^{2}H NMR order parameters measured in 18:0−22:6n3(d_{31})PC with a perdeuterated DHA chain. The double bonds are highlighted with bars and labeled with numbers.

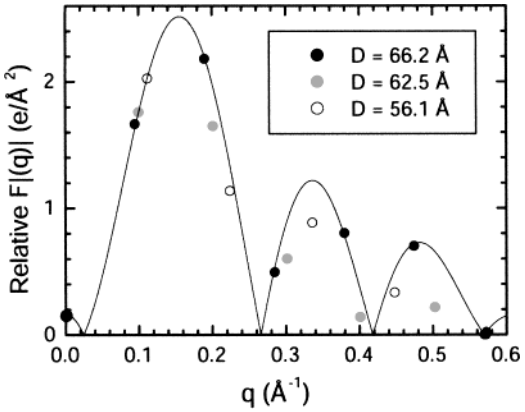

Figure 14. Continuous Fourier transform of 18:0−22:6n3PC calculated as described in Materials and Methods using the D = 66.2 Å data.

this difference, we feel that our value is more accurate since it was confirmed by both ^{2}H and ^{13}C NMR measurements. The order parameters of all DHA/DPA chain segments are significantly lower than the corresponding positions in the saturated sn-1 chains. The lower order in double bonds was expected because of the differences in bond geometry that points the C−H bonds of extended chains at an angle to the bilayer normal close to the magic angle. However, the very low order parameters of all methylene groups between the double bonds can result only from unrestricted chain motions. Remarkably, the methylene groups located between double bonds in DHA (C_6, C_9, C_{12}, C_{15}) have the same very low order parameter of S=0.012. This was confirmed by a magic angle spinning ^{2}H NMR experiment on a perdeuterated DHA chain with chemical shift resolution and scaled recoupling of the quadrupolar splitting.[43] The order of the last methylene group between double bonds, C_{18}, is very low (S = 0.004). Order parameters at C_{21} and C_{22} are also low but slightly higher than C_{16}−C_{20}.

As expected from the relaxation experiments the order parameters of chain segments near the terminal methyl group are particularly low, indicating increased motional amplitudes. The order parameters of chain segments C_{18-21} of DHA and DPA cannot be directly compared due to the lack of double bond number six in DPA. Nevertheless, there is a tendency for, on average, slightly higher order parameters in the olefin range of DPA (see Figure 13). A remarkable feature is that order parameters of carbons in double bonds 1−4 of both DHA and DPA show higher order at the first carbon in the bond relative to the second. The double bonds must be, on average, inclined with respect to the bilayer normal to result in nonequivalent order parameters. This repeating pattern points to structural preferences that are similar for both chains, despite the rapid conversion between conformers. The order parameters of polyunsaturated chains calculated from the simulations are in reasonable agreement with the measured values. Unfortunately, the length of the simulations is still not adequate to report order parameters with sufficiently small error bars that would permit a meaningful quantitative comparison with experimental results.

X-ray Results: The relative continuous Fourier transform calculated for the fully hydrated 18:0(d35)-22:6n3PC is shown in Figure 14. The bilayer structure is best determined from diffuse data such as shown in Figure 1, because the data have been corrected for fluctuation degradation, and also since they extend out to large q values. The form factors at lower D-spacings are added just to check the zeroes shown in Figure 1. These lower D-spacings are too far from full hydration to display diffuse data and so are not fluctuation corrected. As shown, they do not fit neatly onto the continuous transform and were not used for the fully hydrated structure determination. Electron density profiles calculated as described in Materials and Methods of 18:0(d_{35})-22:6n3PC, 18:0(d_{35})-22:5n6PC, and of other lipids for comparison are shown in Figure 15. Profiles

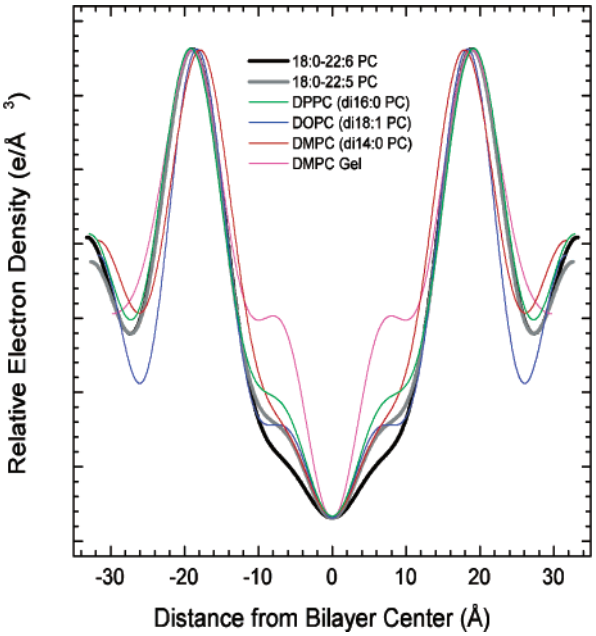

Figure 15. Relative electron density profiles for fluid phase lipids at 24 °C (DOPC and DMPC at 30 °C, DPPC at 50 °C) were constructed from diffuse data such as shown in Figure 1. The DMPC gel phase profile at 10 °C (magenta) was obtained by fitting to a single Gaussian model (see Fig. 9 in ref[40]).

of DOPC, DMPC, and DPPC calculated from diffuse data have not been published previously, but are similar to profiles created by Fourier reconstruction (DOPC,[62] DMPC,[63] and DPPC[64]).

The profiles are arbitrarily normalized to the same peak-to-trough extent. The most prominent feature in a comparison of the profiles is the broader and more shallow methyl trough

(62) Tristram-Nagle, S.; Petrache, H. I.; Nagle, J. F. *Biophys. J.* **1998**, *75*, 917−925.
(63) Petrache, H. I.; Tristram-Nagle, S.; Nagle, J. F. *Chem. Phys. Lipids* **1998**, *95*, 83−94.
(64) Nagle, J. F.; Zhang, R. T.; Tristram-Nagle, S.; Sun, W. J.; Petrache, H. I.; Suter, R. M. *Biophys. J.* **1996**, *70*, 1419−1431.

Table 2. X-ray Results

lipid	*D*-spacing ± 0.2 (Å)	*F*(0) ± 0.04 e/(Å^2)	D_{HH} ± 0.1 (Å)	V_L ± 3 (Å^3)	*A* ± 0.4 (Å^2)	n_w ± 0.5	$2D_c$ ± 0.1 (Å)	$D_{B'}$ ± 0.1 (Å)	k_c ± 0.2 (10^{-12}ergs)	*B* ± 0.2 (10^{12}ergs/cm^4)
18:0-22:6n3PC	66.2	0.16	37.9	1359	68.2	30	30.5	48.5	1.2	1.3
18:0-22:5n6PC	65.2	0.19	37.9	1366	68.7	29.1	30.5	48.5	1.1	2.5

region in the 18:0(d_{35})-22:6n3PC bilayer. By contrast, the profile for 18:0(d_{35})-22:5n6PC is quite similar to the electron density profiles of other lipids such as fluid phase DOPC[62] and DMPC[63] (see Figure 15). This difference between the two profiles of the DHA and DPA lipids extends out to 12 Å from the bilayer center. When we calculate the electron density of each chain minus the terminal methyl group by using a 0.8 ratio for the molecular volumes of CH═CH/CH_2−CH_2,[44] we obtain the chain electron densities: DHA = 0.298 e/ Å^3, DPA = 0.296 e/ Å^3 and stearic acid =0.284 e/ Å^3. The difference in the electron densities of the entire DHA and DPA chain is not significant, but both polyunsaturated chains have a significantly larger electron density than the stearic acid chain. This suggests that the lower electron density seen out to 12 Å from the center of the bilayer in 18:0(d_{35})-22:6n3PC could be due to an increased concentration of the stearic acid chain near the center of the bilayer. The other prominent feature in the profiles is the head-to-head spacing due primarily to the electron dense phosphate groups; this occurs at D_{HH} = 37.9 ± 0.2 Å. The head-to-head spacing is one measure of the bilayer thickness, but perhaps more useful is the value $2D_c$, the thickness of the hydrocarbon core, calculated as in Nagle and Tristram-Nagle, reference 36, $2D_c = 2V_c/A$. This number is 30.5 ± 0.2 Å, in reasonable agreement with the value of 29.6 Å of Petrache et al.[65] who used solid-state ^{2}H NMR together with volume data. We also calculate a thickness parameter, $D_{B'}$, defined in Nagle and Tristram-Nagle,[36,37] which is a more realistic measure of total bilayer thickness since it includes some headgroup water. The value of $D_{B'}$ = 48.5±0.2 Å is the same for both lipids. The surface areas per molecule for 18:0(d_{35})-22:6n3PC and 18:0(d_{35})-22:5n6PC are 68.2 and 68.7 Å^2, respectively, and are identical to within experimental error.

The membranes of both lipids had similar values of the bending modulus $k_c = 1.1-1.2 \times 10\text{-}^{12}$ ergs, slightly higher than 0.8×10^{-12} ergs obtained for DOPC,[62] indicating slightly more rigid bilayers presumably due to the contribution from the saturated chain.[66] The increase in the number of double bonds from five (DPA) to six (DHA) did not alter bilayer elasticity, but may have caused the decrease in the compression modulus *B* (see Table 2) in 18:0(d_{35})-22:6n3PC. The value of *B* reflects the strength of elastic interactions between the bilayers, i.e., the hydration force and the van der Waals interactions.[67] As shown in Table 2, the repeat spacing of bilayers, *D*, was 1 Å larger for 18:0(d_{35})-22:6n3PC compared to 18:0(d_{35})-22:5n6PC, first measured in the oriented samples, and then confirmed using unoriented, fully hydrated capillary samples. Since the bilayer thickness is the same, this indicates slightly larger water spacing between bilayers of 18:0(d_{35})-22:6n3PC, equivalent to a larger number of water molecules/lipid, n_W (see Table 2). We presume that this difference is related to differences in the densities of polyunsaturated chain segments at the lipid water interface that are discussed below.

The remarkable difference between the polyunsaturated lipids in the trough region of electron density profiles can be interpreted by comparison with results from molecular simulations. In Figure 16A the distribution of water, phosphate groups, and of lipid chain segments in units of volume fraction over the bilayer is provided. Within tight error margins both polyunsaturated lipids have identical distributions as expected from X-ray diffraction. However, the distribution of volume densities of saturated and polyunsaturated chains differs substantially over the bilayer (Figure 16B). In both lipids, the density of stearic acid chains is highest in the bilayer center, whereas density of the polyunsaturated chains is higher near the interface. There is an important difference between the lipids: the discrepancy between saturated and polyunsaturated chain densities in the center of the bilayer is significantly smaller for 18:0(d_{35})-22:5n6PC compared to 18:0(d_{35})-22:6n3PC.

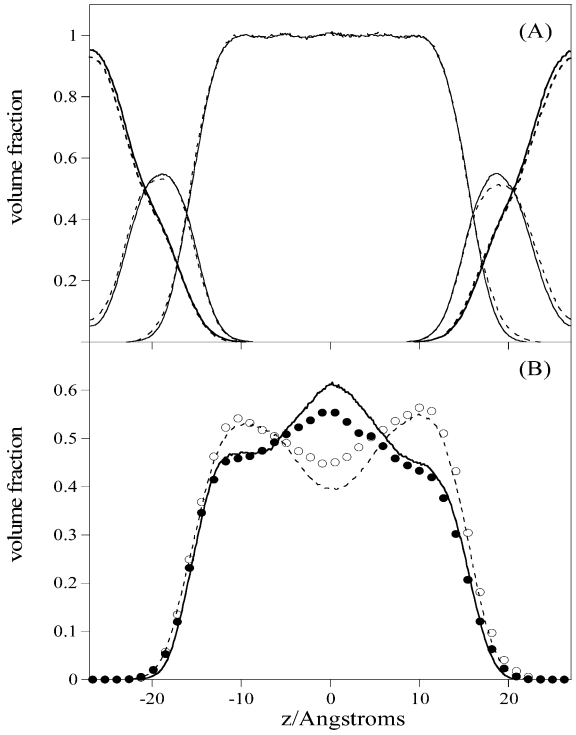

Figure 16. Volume fraction distribution functions in 18:0−22:6n3PC and 18:0-22:5n6PC. (A) The fraction of system volume occupied by water, choline/phosphate/carbonyl groups, and hydrocarbon chains is shown for both lipids (solid—18:0-22:6n3PC, dashed—18:0-22:5n6PC), showing only negligible differences in the overall bilayer structure, (B) The differences between DHA- and DPA-lipids are visible in the fraction of system volume occupied by the sn1 and sn2 fatty acid chains (solid line—stearic acid in 18:0-22:6n3PC, ●—stearic acid in 18:0-22:5n6PC, dashed line—DHA, ○—DPA).

(65) Petrache, H. I.; Salmon, A.; Brown, M. F. *J. Am. Chem. Soc.* **2001**, *123*, 12 611−12 622.
(66) Rawicz, W.; Olbrich, K. C.; McIntosh, T.; Needham, D.; Evans, E. *Biophys. J.* **2000**, *79*, 328−339.
(67) Petrache, H. I.; Gouliaev, N.; Tristram-Nagle, S.; Zhang, R. T.; Suter, R. M.; Nagle, J. F. *Phys. Rev. E* **1998**, *57*, 7014−7024.

This difference, in combination with differences of electron densities between saturated and polyunsaturated chains, and a slightly broader distribution of terminal methyl groups in DHA (data not shown) are responsible for the wider trough in the electron density profile of 18:0(d_{35})-22:6n3PC bilayers.

Discussion

The first reports concerning DHA to DPA replacement under conditions of ω-3 fatty acid starvation were published more than three decades ago.[68] The possibility that changes in membrane properties are responsible for the adverse effects on cell function of this replacement was discussed. Results obtained on less unsaturated membranes, however, suggested that changes in membrane properties caused by the deletion of a single double bond would vanish in highly unsaturated chains. This was frequently cited as evidence that the membrane hypothesis was unlikely to explain the biological effects of ω-3 fatty acid starvation. A definitive study was, until recently, not possible due to the lack of sufficient quantities of purified DPA and because of insufficient resolution in the necessary experimental methods.

Advances in the production of bulk quantities of polyunsaturated fatty acids using algal cultures enabled us to prepare large quantities of DPA with a purity of 98%. Mixed-chain phospholipids with a low level of migration of acyl chains between position sn-1 and sn-2 at the glycerol were subsequently synthesized by Avanti Polar Lipids. Additionally, sample preparation procedures and experimental protocols were developed to monitor and prevent lipid oxidation. With magic angle spinning NMR we resolved a sufficient number of carbon resonances of each polyunsaturated chain to enable a detailed comparison of assigned order parameters and relaxation times. The NOESY proton NMR experiments provided a quantitative measure of conformational disorder and motions of lipids in the bilayers.[23,42,57,69] The diffraction experiments took advantage of recently developed approaches to data analysis in combination with the high intensity of X-rays from a synchrotron beam.[29] Finally, interpretation of differences in lipid packing and dynamics was aided by recent advances in molecular simulations that provided sufficiently accurate and long simulations to calculate correlation functions of dipolar interactions between protons and carbons (to find spin−lattice relaxation times of carbons), and between the protons of lipids (to calculate cross-relaxation rates).[41−43]

Despite the seemingly insignificant difference in chemical structure between the lipids, we observed surprisingly large changes in chain order parameters, spin−lattice relaxation times, effective rates of magnetization transfer from protons to carbons, and, electron density profiles near the center of the bilayer. These differences are not reflected in several parameters traditionally used to compare bilayers: the main phase transition temperature of both lipids is identical within a fraction of a degree centigrade, and overall bilayer geometry, expressed as bilayer thickness and area per molecule, is identical within the margins of experimental error. The outcome of these experiments and simulations points out a difference in the packing of lipid hydrocarbon chains that is represented qualitatively in Figure 17. For 18:0(d_{35})-22:6n3PC the polyunsaturated DHA chain has higher density near the lipid water interface than the saturated stearic acid chain.

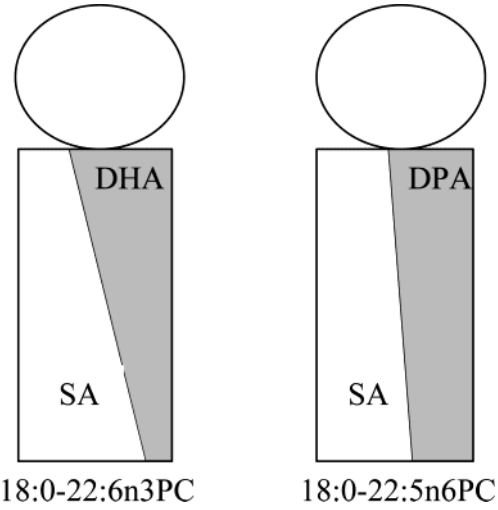

Figure 17. Schematic presentation of the density differences between stearic acid (SA) and the polyunsaturated DHA and DPA chains over the hydrophobic thickness of a monolayer. The volume density of polyunsaturated chains is higher at the lipid water interface, while density of the saturated chain is higher in the bilayer center. The loss of a single double bond from DHA to DPA tends to equalize the differences in chain distributions.

Conversely, in the bilayer center the density of saturated chain segments is higher than the density of DHA. With the loss of a single double bond at the methyl terminal end of the polyunsaturated chain (DHA to DPA replacement) a significant redistribution of chain density takes place. The densities of saturated and polyunsaturated chains at the interface and the bilayer center tend to equalize, whereas the average area per molecule and the hydrophobic thickness of the bilayer are maintained. This model is in agreement with experimental observations. In particular, it predicts differences in the sn-1 chain order profiles with lower order in 18:0(d_{35})-22:6n3PC for carbons C_{10-22} compared to 18:0(d_{35})-22:5n6PC because the stearic acid chain occupies a larger lateral area in the center of the bilayer. However, slightly lower order was also observed for carbons in the region of the order parameter plateau (C_2-C_9) indicating that an increase in area per molecule is not the only reason for changes in sn-1 chain order. The order parameters of the DPA chain compared to DHA are slightly different, in particular for segments near the terminal methyl group, because this chain is on average somewhat more extended than DHA. The difference between electron density profiles is plausible as well: polyunsaturated chains have higher electron density per unit of volume than saturated chains. The relative increase of saturated chain density in the center of 18:0(d_{35})-22:6n3PC bilayers is thus at least partly responsible for the wider trough region.

What could be the reasons for the redistribution of chain densities? The double bonds in polyunsaturated fatty acids are more polarizable than the saturated segments, enabling weak polar interactions between electrical dipoles at the lipid-water interface with polyunsaturated hydrocarbon chains. This difference may be responsible for the higher density of polyunsaturated chains at the lipid water interface compared to saturated and monounsaturated chains. The loss of a double bond near the methyl end of DPA generates a continuous region of five carbons with the interaction properties of a saturated chain. This region is likely to have lower free energy in the bilayer center, exerting a gentle force that stretches the DPA chain. Differences in the distribution of internal degrees of freedom

(68) Morhauer, H.; Holman, R. T. *J. Neurochem.* **1963**, *10*, 523−530.
(69) Yau, W. M.; Gawrisch, K. *J. Am. Chem. Soc.* **2000**, *122*, 3971−3972.

between the polyunsaturated chains, in combination with intermolecular chain-chain interactions, may contribute to the differences in chain distribution as well.

Steric interactions between chains impose an alignment that is reflected in the order parameter profile and in the gradient of correlation times of chain motion. The magnitude of these repulsive steric interactions is a delicate function of the distribution of degrees of freedom over the length of the chain. The differences in the quality and distribution of motional degrees of freedom are well reflected by the spin−lattice relaxation measurements in the center of the bilayer. Both polyunsaturated chains move with larger amplitudes and shorter correlation times than their saturated counterparts, with the DHA chains moving more rapidly than the DPA chains. It is conceivable that the less flexible tail section of DPA favors more extended chain conformations. A theoretical analysis of the influence of polyunsaturation on lipid−lipid interaction may lead to further insight on these observations.

The redistribution of polyunsaturated chain density in going from 18:0(d_{35})-22:6n3PC to 18:0(d_{35})-22:5n6PC is likely to be reflected in the lateral pressure density profiles of their bilayers. Lipid lateral area per molecule is a delicate balance of attractive and repulsive forces. Compression results from the hydrophobic effect at the lipid water interface and attractive van der Waals forces between lipids. Expansion arises from the repulsive steric interactions between the fluid lipid segments. Although attractive and repulsive forces cancel over the thickness of a lipid monolayer, the point of action of these forces is not identical, resulting in a moment of force. If sufficiently large, these forces lead to the bending of monolayers. The X-ray diffraction experiments reveal that the elastic bending modulus of membranes with DHA and DPA chains is identical. Therefore, any possible differences in curvature stress must result from differences in the spontaneous radius of monolayer curvature. Experiments are underway to measure this value. Calculations have indicated that membrane curvature stress can significantly influence the structural equilibrium between conformers of integral membrane proteins with different molecular shape.[70−72] The relationship between membrane curvature and the free energy of protein conformers was explored experimentally for the equilibrium between M_I and M_{II} states of bovine rhodopsin.[73] Because of the significant redistribution of chain densities and its likely effect on the lateral pressure profile, we speculate that the replacement of DHA by DPA has impact on activation of G-protein coupled membrane receptors via curvature stress.

Conformation and Dynamics of Polyunsaturated Chains. The models of polyunsaturated hydrocarbon chains in bilayers have undergone a remarkable transition over the past two decades. Early attempts to find energy minimized structures of polyunsaturated lipids[74−76] inadvertently contributed to the perception that polyunsaturated chains in membranes are rigid and bulky. The lower order parameters/faster dynamics of unsaturated chains and of labels in polyunsaturated lipid matrixes were thought to be related to packing perturbations from the introduction of bulky polyunsaturated chains. However, our more recent experiments and simulations,[43,45,55,77−81] as well as those from other laboratories (see e.g., refs 58,61,65,82−84), allow us to conclude that polyunsaturated chains surpass their saturated and monounsaturated counterparts in conformational freedom and in the rate of structural transitions, particularly for the segments near the terminal methyl group. The amplitudes and correlation times of motions of polyunsaturated chains are close to those in neat liquids. This exceptional flexibility is related to the electronic structure of polyunsaturated chains. Although these chains have fewer degrees of freedom, their flexibility is greatly promoted by lower potential energy barriers for rotation about C−C single bonds.[43] Low concentrations of polyunsaturated lipids, in the range from 1 to 10 mol %, are found in the majority of lipid matrixes of mammals. Although the changes in global membrane properties are less pronounced at low concentrations, these lipids may nevertheless influence the function of integral proteins. It is conceivable that the ease at which the polyunsaturated chains change their conformations allows these chains to adapt to the rugged surface of transmembrane helix bundles. Additionally, the polarity of the double bonds may enable them to engage in polar interactions with the electrical dipoles in transmembrane helices. Thus the DHA chains seem ideally suited to "solvate" integral membrane proteins, in particular those that undergo rapid structural transitions. The differences in conformational freedom and dynamics between DHA and DPA would likely have an impact on protein function and thus explain the adverse effects observed upon fatty acid replacement.

Acknowledgment. The purification of DPA by preparative HPLC was conducted by Joby Mathews. Dr. Laura L. Holte conducted the ^{13}C-^{13}C COSY experiment on a sample of ^{13}C-labeled DHA that was kindly provided by Martek Biosciences. The authors thank Dr. John F. Nagle and Yufeng Liu for assistance in obtaining the X-ray data, and Yufeng Liu for providing the diffuse scattering analysis program. S. E. F. thanks the National Science Foundation for support through award MCB-009150 S.T.-N. thanks the NIH for support through Grant No. GM44976 and for use of the CHESS synchrotron through NSF Grant No. DMR-9311772.

Supporting Information Available: ^{31}P NMR spectra of 18:0(d_{35})-22:6n3PC and 18:0(d_{35})-22:5n6PC; ^{1}H- and ^{13}C MAS NMR spectra of 18:0(d_{35})-22:5n6PC; ^{1}H chemical shift assignments and spin−lattice relaxation times of 18:0−22:6n3PC, 18:0(d_{35})-22:6n3PC, and 18:0(d_{35})-22:5n6PC; intensities of diagonal- and cross-peaks of 18:0(d_{35})-22:5n6PC as a function of mixing time; NOESY cross-relaxation rate matrices of 18:0(d_{35})-22:6n3PC and 18:0(d_{35})-22:5n6PC. This material is available free of charge via the Internet at http://pubs.acs.org.

JA029029O

(70) Gruner, S. M.; Shyamsunder, E. *Ann. N. Y. Acad. Sci.* **1991**, *625*, 685−697.
(71) Cantor, R. S. *Chem. Phys. Lipids* **1999**, *101*, 45−56.
(72) Cantor, R. S. *J. Phys. Chem. B* **1997**, *101*, 1723−1725.
(73) Botelho, A. V.; Gibson, N. J.; Thurmond, R. L.; Wang, Y.; Brown, M. F. *Biochemistry* **2002**, *41*, 6354−6368.
(74) Applegate, K. R.; Glomset, J. A. *J. Lipid Res.* **1991**, *32*, 1635−1644.
(75) Applegate, K. R.; Glomset, J. A. *J. Lipid Res.* **1991**, *32*, 1645−1655.
(76) Applegate, K. R.; Glomset, J. A. *J. Lipid Res.* **1986**, *27*, 658−680.
(77) Separovic, F.; Gawrisch, K. *Biophys. J.* **1996**, *71*, 274−282.
(78) Huster, D.; Jin, A. J.; Arnold, K.; Gawrisch, K. *Biophys. J.* **1997**, *73*, 855−864.
(79) Huster, D.; Arnold, K.; Gawrisch, K. *Biochemistry* **1998**, *37*, 17 299−17 308.
(80) Binder, H.; Gawrisch, K. *Biophys. J.* **2001**, *81*, 969−982.
(81) Binder, H.; Gawrisch, K. *J. Phys. Chem. B* **2001**, *105*, 12 378−12 390.
(82) Saiz, L.; Klein, M. L. *J. Am. Chem. Soc.* **2001**, *123*, 7381−7387.
(83) Saiz, L.; Klein, M. L. *Biophys. J.* **2001**, *81*, 204−216.
(84) Rabinovich, A. L.; Ripatti, P. O. *Biochim. Biophys. Acta* **1991**, *1085*, 53−62.